AIP Physics of Plasmas

Thrust and efficiency model for electron-driven magnetic nozzles

Justin M. Little and Edgar Y. Choueiri

Citation: Phys. Plasmas **20**, 103501 (2013); doi: 10.1063/1.4824613
View online: http://dx.doi.org/10.1063/1.4824613
View Table of Contents: http://pop.aip.org/resource/1/PHPAEN/v20/i10
Published by the AIP Publishing LLC.

PHYSICS OF PLASMAS **20**, 103501 (2013)

Thrust and efficiency model for electron-driven magnetic nozzles

Justin M. Little[a)] and Edgar Y. Choueiri
Electric Propulsion and Plasma Dynamics Laboratory, Princeton University, Princeton, New Jersey 08544, USA

(Received 1 May 2013; accepted 23 September 2013; published online 11 October 2013)

A performance model is presented for magnetic nozzle plasmas driven by electron thermal expansion to investigate how the thrust coefficient and beam divergence efficiency scale with the incoming plasma flow and magnetic field geometry. Using a transformation from cylindrical to magnetic coordinates, an approximate analytical solution is derived to the axisymmetric two-fluid equations for a collisionless plasma flow along an applied magnetic field. This solution yields an expression for the half-width at half-maximum of the plasma density profile in the far-downstream region, from which simple scaling relations for the thrust coefficient and beam divergence efficiency are derived. It is found that the beam divergence efficiency is most sensitive to the density profile of the flow into the nozzle throat, with the highest efficiencies occurring for plasmas concentrated along the nozzle axis. Increasing the expansion ratio of the magnetic field leads to efficiency improvements that are more pronounced for incoming plasmas that are not concentrated along the axis. This implies that the additional magnet required to increase the expansion ratio may be worth the added complexity for plasma sources that exhibit poor confinement. [http://dx.doi.org/10.1063/1.4824613]

I. INTRODUCTION

Simply stated, a magnetic nozzle (MN) converts random thermal energy of a plasma into directed kinetic energy. This conversion occurs as the plasma expands through a cylindrically symmetric magnetic field that is contoured similarly to the solid walls of a conventional rocket nozzle (see Fig. 1). Momentum imparted to the accelerated plasma is transferred back to the MN through the repulsion of the magnetic circuit and internal plasma currents. Applications include laboratory simulations of space plasmas,[1] surface processing,[2] and plasma propulsion for spaceflight.[3–22]

MNs have been envisioned as the acceleration stage for a diverse number of space propulsion concepts ranging from 50 W thrusters[14] to 1 GW Fusion rockets.[21] Their ability to scale to high powers is largely due to their independence from electrodes, whose erosion typically limits the lifetime of high-power thrusters.[23] Other benefits include magnetic shielding of solid surfaces from high energy particles (recently observed to significantly decrease the erosion of Hall thruster channels),[24–26] a quasi neutral exhaust beam, and the ability to use various propellants.[27] The main challenges to the efficacy of MNs for space propulsion are poor ionization and excessive losses at low powers and magnetic fields,[7] and plasma detachment from the applied magnetic field.[28–32]

The low densities and high temperatures within a typical MN plasma frequently prevent thermal equilibrium among the various species.[22] Oftentimes, the energization stage of the upstream plasma source targets a single species (e.g., resonant wave heating). As a result, the plasma expansion dynamics will be driven primarily by the species that possesses the highest temperature.[33,34]

An electron-driven magnetic nozzle (ED-MN), the focus of this paper, is characterized by the flow of a hot electron, cold ion plasma ($T_e \gg T_i$) through a convergent-divergent magnetic field topology. The electrons, by virtue of their temperature, naturally expand through the nozzle at a rate greater than the ions. The tendency of the plasma to remain globally quasineutral leads to the formation of an ambipolar electric field,[4,5] and under certain circumstances a current-free double layer (CFDL)[35–38] or quasineutral steepened layer (QSL),[8,9] which accelerates the cold ion population.[19,39] Confinement of the thermal electrons by the applied magnetic field induces an azimuthal current density, or electron diamagnetic current, which is the primary mechanism of momentum transfer between the plasma and nozzle.[3,6,16,31]

A. Motivation for an ED-MN performance model

ED-MNs are commonly found as the acceleration stage of wave-produced plasma propulsion concepts, e.g., electron-cyclotron-resonance (ECR)[10–12] and helicon thrusters.[13–18] In contrast to the generalized MN field geometry of Fig. 1, expansion and acceleration of the plasma typically occur in the fringe field of the plasma source magnets. For a fully ionized argon plasma with an electron temperature of 10 eV, input power of 1 kW, 50% thrust efficiency, and thrust coefficient (defined later) of 4, these devices have the potential to operate near a specific impulse (I_{sp}) of 2000 s with 50 mN of thrust.

Direct thrust stand measurements of helicon thrusters have recently been used to verify the generation of thrust,[15–18] observe force coupling between diamagnetic plasma and electromagnet currents,[16] and characterize the performance over a wide operational parameter space.[17,18] These thrust measurements, typically between 1 and 10 mN/kW, demonstrate specific impulse values in the range of 100–500 s with thrust efficiencies near 1%.

[a)]jml@princeton.edu. URL: http://alfven.princeton.edu

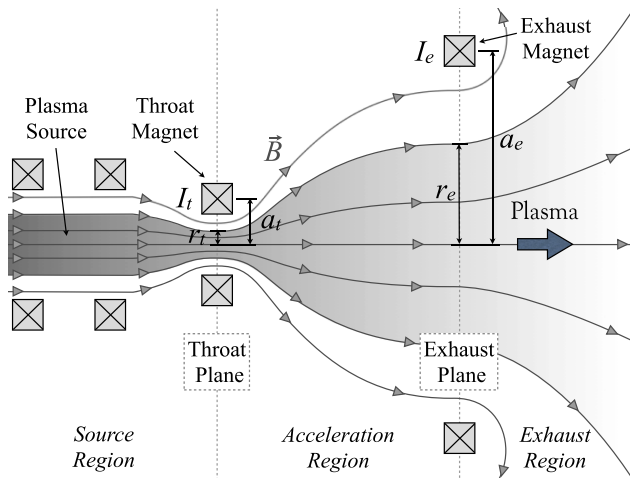

FIG. 1. Example of a magnetic nozzle configuration. Solid gray lines represent the surfaces of constant magnetic flux along which the magnetic field vector, $\vec{B}$, is tangential.

Clearly, a deeper understanding of the loss processes inside the plasma source and through the expansion region is required if thrusters that utilize ED-MNs are to reach their potential and become competitive with established electric propulsion devices within a similar class (10^2–10^4 W).

Assuming the plasma is singly ionized, the specific impulse may be written as $I_{\rm sp} \approx \eta_m I_{\rm sp}^{i,e}$. Here, $\eta_m = \dot{m}_i/\dot{m}$ is the propellant mass utilization efficiency and $I_{\rm sp}^{i,e}$ is the specific impulse contribution from the ions and electrons. The thrust contribution of the neutral gas is assumed to be negligible due to low temperatures and pressures.[16]

We define the thrust coefficient as the thrust normalized by the pressure force at the nozzle throat. The thrust coefficient relates to the specific impulse and the ion acoustic speed at the nozzle throat, $c_s = \sqrt{T_e/m_i}$, through $C_T = g_0 I_{\rm sp}^{i,e}/c_s$. A normalized specific impulse may then be defined such that,

$$\hat{I}_{\rm sp} \equiv \frac{g_0 I_{\rm sp}}{c_s} = \eta_m C_T. \tag{1}$$

We will later show that C_T typically takes values between 2 and 7 and depends mainly on the MN geometry. Equation (1) demonstrates the known influence of the mass utilization efficiency on the specific impulse. This has been experimentally shown to be the primary cause of the poor I_{sp}-performance of ED-MN thrusters.[15,18]

The thrust efficiency, η, is classically defined[40] as

$$\eta = \frac{F^2}{2\dot{m}P_{\rm tot}}, \tag{2}$$

where F is the thrust, $\dot{m}$ is the total mass flow rate, and $P_{\rm tot}$ is the total input power. It may be expressed as the product of a beam divergence efficiency ($\eta_{\rm div}$) and plasma source internal efficiency ($\eta_{\rm int}$): $\eta = \eta_{\rm div}\eta_{\rm int}$.[41] Here, $\eta_{\rm div}$ is the ratio of the directed to undirected kinetic power of the exhaust beam and $\eta_{\rm int}$ accounts for losses associated with coupling between the power supply and plasma, ionization and excitation of the propellant, radiation, and particle transport to the walls of the thruster.

The plasma source influences η_m and $\eta_{\rm int}$,[41] while the MN controls $\eta_{\rm div}$ and C_T.[6] Thus, the specific impulse and thrust efficiency of an ED-MN thruster depend on parameters inherent to either the plasma source or the MN. It is, therefore, possible to separate the performance of the plasma source from that of the ED-MN when developing thrust and efficiency models.

The properties of the source plasma are likely to depend on the mass flow rate, source geometry, magnetic field strength and geometry, input power, ionization mechanism, and operation mode.[42–44] Therefore, performance modeling of the plasma source is difficult to generalize even among this restricted class of magnetic nozzle thrusters. Models have been put forth to explain the power balance within ECR[2] and helicon thrusters.[41] The addition of geometric effects and wave physics has proven to be difficult, however.

Fortunately, the nature of plasma flow through the MN is more amenable to a general analytical model. Thus, the question that we will address in this paper is the following: how does the beam divergence efficiency, $\eta_{\rm div}$, and thrust coefficient, C_T, of an electron-driven magnetic nozzle scale with the properties of the incoming plasma flow and magnetic field geometry?

B. Previous ED-MN models

Andersen *et al.*[45] used a quasi-one-dimensional (Q1D) model to analyze experimental data that showed ion acceleration through a MN. Modifications to this model have included disparate ion and electron temperatures,[46] ionization,[2] recombination,[47] neutral collisions,[48] CFDLs,[37] and electron kinetic effects.[49]

Q1D models are limited by the fact that any variation of the plasma parameters in the direction perpendicular to the flow is averaged out. Therefore, it is impossible to predict the effect of non-uniformities in this direction. Some semi-empirical performance models have had success by assuming that the radial plasma density profile maintains the same shape, or is self-similar, throughout the exhaust.[16,48] The self-similar assumption, however, is not capable of describing the radial focusing of the plasma density profile with respect to the magnetic field divergence: a behavior that has been observed in several experiments[4,13,50,51] and numerical models.[6,13]

Ahedo and Merino investigated the 2D nature of ED-MNs by numerically solving the collisionless two-fluid plasma equations.[6] They showed that the relative focusing of the density profile occurs along with the growth of an electric field perpendicular to the direction of the applied magnetic field. They also observed separation between the ion and electron (magnetic) streamlines. A later extension of their numerical model to the far downstream region revealed that ion separation from the magnetic field lines results in the bulk flow of momentum towards the downstream direction, thus minimizing the problem of plasma detachment, and allowing for the determination of $\eta_{\rm div}$ and C_T.[52]

Numerical models have provided valuable insight into the 2D nature of ED-MN exhaust plumes, but a simple performance model that captures this nature is lacking. Because

of its ability to self-consistently reproduce 2D effects, we seek an approximate, fully analytical solution to the model of Ahedo and Merino. We derive in Sec. II a general solution to the two-fluid equations for a collisionless, magnetized plasma flow with $T_e \gg T_i$. In Sec. III, we apply this solution to the ED-MN exhaust plume and compare the analytical solution to the numerical results of Ahedo and Merino. The transparency of our analytical solution allows us in Sec. IV to analyze in greater depth than possible with numerical solutions the dependence of the 2D nature of the plasma exhaust on the properties of the plasma flow into the MN. This analysis ultimately yields analytical scaling laws for η_{div} and C_T in terms of the properties of the plasma flow into the MN and magnetic field geometry.

II. TWO-FLUID MODEL SEPARABLE SOLUTION

In this section, we derive an approximate analytical solution to the two-fluid model proposed by Ahedo and Merino.[6] Our solution is motivated by their numerical results, which indicate that the average of the plasma potentials along the nozzle axis and the exhaust boundary approximates the potential predicted from the Q1D model. Assuming that the ion trajectory *approximately* follows the magnetic field lines, it is possible to find the potential gradient in the direction perpendicular to the magnetic field. This result, combined with the Q1D solution for the potential averaged over the plasma cross-section, yields an analytical expression for the 2D potential distribution in the plasma. Conservation equations provide the plasma density and ion Mach number.

A. Governing equations

We restrict our model to an isothermal, collisionless plasma flow. The isothermal electron assumption is common in the literature due to the high electron thermal conductivity along the magnetic field.[2] The validity of the collisionless assumption depends strongly on the properties of the source plasma, but is typically met in low-pressure, high-temperature ED-MN plasmas.[22]

The model also neglects electron inertial effects and induced magnetic fields. Electron inertial effects become important when $r_{L,e}/L_{\nabla B} \sim 1$, where $r_{L,e}$ is the electron Larmor radius and $L_{\nabla B} = |B/\nabla B|$ is the magnetic field scale length. The magnitude of the induced magnetic field becomes the same order as the applied magnetic field as $\beta \sim 1$. Here, β is the ratio of the thermal energy density of the plasma to the magnetic field energy density. These requirements ($r_{L,e}/L_{\nabla B} \ll 1$ and $\beta \ll 1$) are met in a typical ED-MN plasma source.[22] Far downstream, however, both $r_{L,e}/L_{\nabla B}$ and β may approach unity,[22] at which point these processes have been hypothesized to play a pivotal role in plasma detachment.[29–32]

In light of the above assumptions, the problem is described by the momentum and continuity equations for the ions and electrons.[6] These eight equations may be re-cast in the following dimensionless form:

$$\nabla\left(\frac{1}{2}u_i^2 + \phi\right) = \mathbf{u}_i \times \left(\frac{\mathbf{B}}{\rho_i} + \nabla \times \mathbf{u}_i\right), \tag{3}$$

$$\nabla(\ln n - \phi) = \mathbf{u}_e \times \frac{\mathbf{B}}{\rho_e}, \tag{4}$$

$$\nabla \cdot (n\mathbf{u}_i) = 0, \tag{5}$$

$$\nabla \cdot (n\mathbf{u}_e) = 0. \tag{6}$$

Here, we have normalized the ion and electron velocities by the ion acoustic speed, $c_s = (k_b T_e/m_i)^{1/2}$. The electric potential, Φ, is normalized by the electron temperature, T_e, such that $\phi = e\Phi/kT_e$. Furthermore, $\rho_j = (m_j c_s/eB^*)/L^*$ is the normalized Larmor radius of species j, with B^* and L^* the characteristic magnetic field strength and length scale of the plasma, respectively. We note ρ_i represents an *effective* Larmor radius for the ions, and can be viewed as a measure of ion magnetization.[6]

B. Quasi-field-aligned approximation

Using an approximation for the ion trajectory, we will now reduce Eqs. (3)–(6) to a system of three equations for three unknowns: the ion Mach number, $M = |\mathbf{u}_i|$; the plasma density, n; and the plasma potential, ϕ.

First, we consider the component of Eq. (4) along the magnetic field unit vector, $\mathbf{b}$,

$$\mathbf{b} \cdot \nabla(\phi - \ln n) = 0. \tag{7}$$

This is the well-known Boltzmann relation.[53]

Ahedo and Merino[6] show that the terms on the right hand side of Eq. (3) have little influence on the ion dynamics for flows that satisfy $\rho_i \ll 1$. The triviality of this term, which includes the centrifugal and magnetic forces, implies that the ion motion is dominated by electrostatic forces. Furthermore, they find $M \gg |\mathbf{u}_i \cdot \mathbf{e}_\theta|$, which implies the ion velocity unit vector, $\mathbf{s}$, is contained primarily in the r–z plane: $\mathbf{s} \cdot \mathbf{e}_\theta \approx 0$.

Projecting Eq. (3) onto the ion velocity unit vector relates the ion Mach number and potential,

$$\mathbf{s} \cdot \nabla(M^2 + 2\phi) = 0, \tag{8}$$

which represents the conservation of ion energy along an ion streamline.

The final equation comes from rewriting Eq. (5) in integral form. Applying the divergence theorem yields,

$$\int_S nM(\mathbf{s} \cdot \mathbf{dA}) = 0, \tag{9}$$

where S denotes the control surface.

Equations (7)–(9) represent an underdetermined system of three equations for four unknowns: M, n, ϕ, $\mathbf{s}$. The only physical phenomena eliminated from the governing equations, Eqs. (3)–(6), are the magnetic and centrifugal forces on the ions. Closure of the problem does not require the equation for electron force balance in the perpendicular direction as it would introduce the electron azimuthal velocity, $u_{\theta,e}$, as a fifth unknown. In fact, assuming knowledge of the plasma parameters along a cross-sectional flow plane, $u_{\theta,e}$ is uniquely determined everywhere by only the magnetic field topology.[32]

Numerical results[6] indicate that, even for plasmas where the ion streamlines deviate significantly from their initial magnetic flux surface, the local angle between the magnetic field and ion velocity unit vectors remains less than 5° even far downstream into the plume. Thus, we close the system of equations by assuming that ion velocity unit vector is *approximately* parallel to the magnetic field unit vector, $\mathbf{s} \approx \mathbf{b}$. We refer to this assumption as *quasi*-field-aligned flow.

While the quasi-field-aligned approximation seems prohibitive, especially in the presence of significant cross-field ion motion, we will show in Sec. III that it allows analytical solutions that exhibit remarkable agreement with numerical solutions. Eventually, however, this approximation becomes invalid in the far-field region beyond the turning point of the magnetic field.[52]

C. Coordinate transformation

With the aim of further simplifying Eqs. (7)–(9), we employ a transformation from cylindrical to magnetic coordinates.[54]

The magnetic field vector, $\mathbf{B}$, may be described in terms of two scalar functions as

$$\mathbf{B} = -\frac{1}{r}(\mathbf{e}_\theta \times \nabla\psi) = -\nabla\zeta, \tag{10}$$

where ψ is constant along any magnetic flux surface, ζ is constant along any surface that is everywhere normal to the magnetic field vector, and $\mathbf{e}_\theta$ is the unit vector in the azimuthal direction. We will refer to surfaces of constant ψ and ζ as ψ-surfaces and ζ-surfaces, respectively. Figure 2 illustrates the conversion from cylindrical coordinates to magnetic coordinates for a plasma flow contained within the flux surface ψ_p.

The coordinate transformation allows the simplification, $\mathbf{b} \cdot \mathbf{dA} = dA$, where dA is the differential area of a ζ-surface. The integral of a function $X(\psi, \zeta)$ over a ζ-surface from $\psi \in [0, \psi_p]$ simplifies to

$$\int_\zeta X(\psi,\zeta)dA = 2\pi\int_0^{\psi_p} \frac{X(\psi,\zeta)}{B(\psi,\zeta)}d\psi. \tag{11}$$

Furthermore, the ψ-average of this function is given by

$$\bar{X}(\zeta) = [A(\zeta)]^{-1}\int_\zeta X(\psi,\zeta)dA, \tag{12}$$

where $A(\zeta)$ is the total area of the ζ-surface.

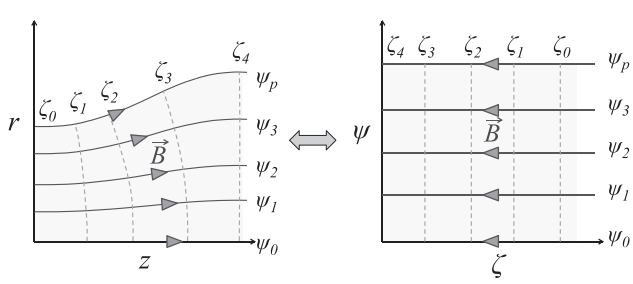

FIG. 2. Transformation from cylindrical (r, z) to magnetic (ψ,ζ) coordinates. $\vec{B}$ represents the magnetic field vector aligned along surfaces of constant ψ.

D. Throat plane

We now assume that there exists a throat plane defined by $\zeta = \zeta_t$, along which $M(\psi, \zeta_t) = 1$ and $\phi(\psi, \zeta_t) = 0$. The plasma density profile along this plane is defined by the function $n(\psi, \zeta_t) = n_t(\psi)$.

Using the quasi-field-aligned assumption, the conditions at the throat plane may be substituted into Eqs. (7) and (8) to yield algebraic expressions for the density and ion Mach number in terms of the electric potential,

$$n = n_t e^{\phi}, \tag{13}$$

$$M = \sqrt{1 - 2\phi}. \tag{14}$$

Thus, our main task is to derive ϕ, from which n and M may be found from Eqs. (13) and (14).

E. Separable solution

The coordinate transformation presented in Sec. II C enables the separate treatment of the electric potential averaged over the beam cross-section and its variation across the beam cross-section,

$$\phi(\psi,\zeta) = \bar{\phi}(\zeta) + \varphi(\psi,\zeta), \tag{15}$$

with the additional requirement

$$\int_\zeta \varphi(\psi,\zeta)dA = 0. \tag{16}$$

Hence, along each ζ-surface, the potential is separated into a ψ-averaged component, $\bar{\phi}$, and a two-dimensional, ψ-dependent correction, ϕ, whose average over the entire beam cross-section along the ζ-surface is zero.

The ζ-dependence of the ψ-averaged potential is obtained from the well known Q1D model,[45]

$$e^{\bar{\phi}}\sqrt{1 - 2\bar{\phi}} = \frac{A_t}{A}. \tag{17}$$

Here, $A_t = A(\zeta_t)$ may be found from Eq. (11). We note that Eq. (17) is an implicit equation and does not have a closed-form solution.

The ψ-dependent correction, ϕ, may be found from the force balance on ions in the direction perpendicular to the magnetic field,

$$rB\frac{d\varphi}{d\psi} = -\frac{M^2}{R_c}. \tag{18}$$

We have introduced here the local radius of curvature of the ion streamline, $R_c = |\mathbf{n} \cdot (\mathbf{s} \cdot \nabla\mathbf{s})|^{-1}$, where $\mathbf{n}$ is the unit vector along a ζ-surface.

Invoking the quasi-field-aligned approximation, we express the radius of curvature in terms of the unit vectors perpendicular and parallel to the applied magnetic field, $\mathbf{h}$ and $\mathbf{b}$, respectively: $R_c \approx |\mathbf{h} \cdot (\mathbf{b} \cdot \nabla\mathbf{b})|^{-1}$. This allows R_c to be determined from the local radius of curvature of the applied magnetic field.

Substitution of Eqs. (14) and (15) into Eq. (18) allows the description of φ in terms of the nonlinear ordinary differential equation,

$$\frac{d\varphi}{d\psi} + \frac{1 - 2\bar{\phi} - 2\varphi}{rBR_c} = 0, \tag{19}$$

from which separation of variables and Eq. (15) yield

$$\phi(\psi, \zeta) = \frac{1}{2} + C(\zeta)\exp\left[\int_0^{\psi} K(\psi', \zeta)d\psi'\right]. \tag{20}$$

Here, $K = (rBR_c)^{-1}$, and represents the effective local curvature of the magnetic field in the magnetic coordinate system. The integration constant, C, may be found from Eq. (16).

We take a moment to discuss an inconsistency that arises from solving Eq. (18) with the quasi-field-aligned approximation. Specifically, the formation of a perpendicular electric field implies a changing cross-sectional density profile through Eq. (13). However, the changing density profile requires that the ion streamlines deviate from the magnetic field lines to preserve quasineutrality. The implication is that perpendicular electric fields are incapable of constraining ions to *exactly* follow curved magnetic field lines.

Therefore, the quasi-field-aligned approximation is inconsistent with Eq. (18) because the local ion curvature radius cannot equal the magnetic field curvature radius. By setting the two curvature radii to be equal, Eq. (18) overestimates the electric field, and thus also the potential gradient in the cross-field direction. We will show, however, that the error due to this inconsistency is relatively small for plasma flows through slowly diverging magnetic fields. This is because the cross-field velocity of the ions remains small compared to the field-aligned velocity, which implies that the length scale of separation between the ion streamlines and magnetic field lines is much smaller than the length scale over which that separation occurs. Ultimately, this allows our analytical solution to capture the effect of ion cross-field motion on the plasma density profile without consistently solving the ion equations of motion.

F. Mass conservation

Using the expansion region of an ED-MN plasma as an example, we will show in Sec. III that the analytical equations derived in Sec. II E predict ϕ, M, and $\ln(n)$ to within a few percent of the values obtained from the numerical solution to the fluid equations. However, the error in ϕ increases in the far downstream region due to ion cross-field motion. Because errors in n scale exponentially with errors in ϕ, the separable solution violates mass conservation in this region. To determine the nozzle thrust coefficient, C_T, it is necessary to implement a mass conservation correction into the solution.

The excess mass flow rate through each ζ-surface is given by

$$\epsilon_{\dot{m}} = \frac{1}{\bar{n}_t A_t}\int_{\zeta} nMdA, \tag{21}$$

where zero error occurs for $\epsilon_{\dot{m}} = 1$. We multiply each plasma parameter by a correction factor, α, that is a function of only ζ, such that,

$$\phi \to \alpha_\phi \phi, \quad n \to \alpha_n n, \quad M \to \alpha_M M. \tag{22}$$

Using Eq. (21), mass conservation is guaranteed for any α-combination that satisfies

$$\epsilon_{\dot{m}} = (\alpha_M \alpha_n)^{-1}. \tag{23}$$

The mass-conserving solutions must also satisfy the quasi-one-dimensional equations. From these, we derive the final two equations needed to solve for each α

$$(1 - 2\bar{\phi})\exp[2(1 - \alpha_\phi)\bar{\phi}] - \epsilon_{\dot{m}}^2(1 - 2\alpha_\phi\bar{\phi}) = 0, \tag{24}$$

$$\alpha_n = \exp[(\alpha_\phi - 1)\bar{\phi}], \tag{25}$$

Here, $\bar{\phi}$ is the ψ-averaged potential *prior* to applying the mass correction. Equation (24) represents an implicit equation for α_ϕ in terms of $\bar{\phi}$ and $\epsilon_{\dot{m}}$. The mass-conserving potential may then be found by multiplying the right hand side of Eq. (20) by α_ϕ.

III. ELECTRON-DRIVEN MAGNETIC NOZZLE FLOW

We will now demonstrate how our 2D separable solution can be applied to the exhaust plume of an ED-MN plasma. Most experiments and physical models of MNs use a simple magnetic configuration for which acceleration occurs in the fringe fields of the plasma source magnets. We will not restrict ourself to this configuration, but rather allow for an acceleration region prior to the exhaust plane as depicted in Fig. 1. Ultimately, this is equivalent to starting the model of Ahedo and Merino[6] with a Mach number greater than one.

A. Magnetic field model

We begin by defining the coordinate transformation from cylindrical to magnetic coordinates (Figure 3). The magnetic field in the exhaust region may be approximated by the magnetic field of a single loop of current, from which the ψ-surfaces[29] and ζ-surfaces may be further approximated as

$$\psi(r, z) = \frac{r^2/2}{(1 + r^2 + z^2)^{3/2}}, \tag{26}$$

$$\zeta(r, z) = \frac{z/2}{(r^2 + z^2)^{3/2}}. \tag{27}$$

All lengths above and throughout the remainder of the paper are normalized by the effective radius of the exhaust magnet, a_e. Equation (27) is a valid approximation to Eqs. (10) and (26) for values of $z > 1$. From this point forward, our results will be limited to MN exhausts whose magnetic field may be approximated by that of a dipole, or Eqs. (26) and (27).

The specific magnetic field topology in the acceleration region is peripheral if we assume the following: (1) the plasma remains self-similar in the acceleration region and (2) the flow is field-aligned and directed along the nozzle axis at the exhaust plane ($B_r \approx u_r \approx 0$). The first requirement implies,

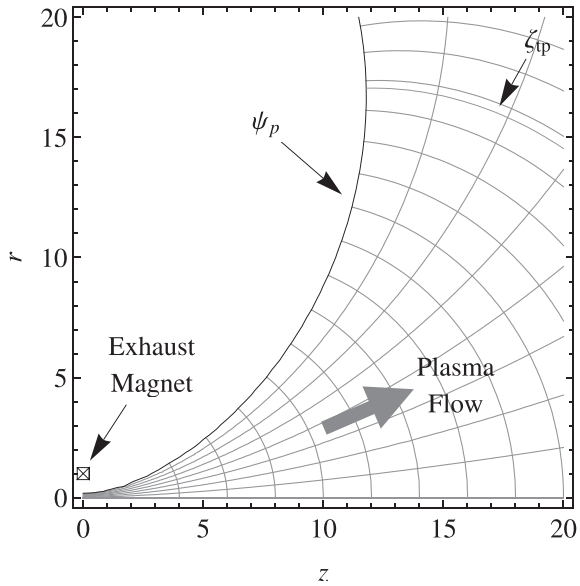

FIG. 3. Transformation from cylindrical (r, z) to magnetic (ψ, ζ) coordinates using Eqs. (26) and (27). Distances are normalized by the effective radius of the exhaust magnet, a_e. In this example, the bounding flux surface is given by $\psi_p = \psi(0.185, 0)$. The ζ-surface corresponding to the turning point (tp) of ψ_p is labelled ζ_{tp}.

$$(R_E R_{A,t})^{1/2} < \frac{l_e}{a_t} < \frac{2}{30 R_{A,t}},$$

where l_e is the distance between the exhaust and throat magnets. We define the expansion ratio, $R_E = (r_e/r_t)^2$, and throat aperture ratio, $R_{A,t} = (r_t/a_t)^2$. The first inequality promotes flow stability by limiting the magnetic field curvature in this region,[56] while the second inequality is required for self-similarity (see Sec. III C).

B. Acceleration region

The acceleration region, used to increase the Mach number of the flow prior to entering the exhaust region, relates the throat and exhaust plane plasma parameters. For the magnetic field model above, the throat is not necessarily located at $z = 0$, but rather at some unspecified location upstream the exhaust plane. Along the throat plane, the potential and ion Mach number are given by $M(\psi, \zeta_t) = 1$ and $\phi(\psi, \zeta_t) = 0$, respectively.

An analytical expression for the radial density distribution of plasma confined within a cylindrical vessel was derived by Ahedo,[55] and later used by Ahedo and Merino[6] to characterize the 2D expansion of a non-uniform magnetic nozzle plasma. To allow direct comparison with their numerical results, we adopt their expression and transform it to magnetic coordinates as

$$n(\psi, \zeta_t) = J_0\left[a_0 \sigma \left(\frac{2\psi^{1/2} + 3\psi^{3/2}}{2\psi_p^{1/2} + 3\psi_p^{3/2}}\right)\right]. \tag{28}$$

In this equation, J_0 is the zeroth Bessel function, a_0 is the first zero of J_0, and σ is a parameter less than unity that controls the uniformity of the density profile at the throat. For example, $\sigma = 0$ represents a radially uniform plasma. The uniformity decreases for $\sigma > 0$.

The plasma at the nozzle exhaust plane is related to the throat plane by two geometric ratios: the expansion ratio, R_E, and exhaust aperture ratio, $R_{A,e}$. The expansion ratio, defined above, determines the Mach number at the exhaust plane, M_e, through Eq. (14),

$$R_E = \frac{1}{M_e} \exp\left(\frac{M_e^2 - 1}{2}\right). \tag{29}$$

The exhaust aperture ratio, $R_{A,e} = (r_e/a_e)^2$, determines the bounding magnetic field flux surface, $\psi_p = \psi(r_e, 0)$, and thus the divergence of the plasma boundary in the exhaust region. It is no surprise at this point that M_e, r_e, and σ will ultimately be used as the independent variables of the ED-MN performance model.

C. Analytical solution

Armed with a magnetic field model (Sec. III A) and exhaust plane conditions (Sec. III B), our task is now to solve Eq. (20) for ϕ.

Substitution of Eq. (26) into Eq. (10) yields an expression for **B**. This expression may then be inserted into Eq. (11) with $X = 1$ to find the cross-sectional area, A. The area of the plasma at ζ_t is given by $A_t = A_e/R_E = \pi r_e^2/R_E$. Finally, insertion of the ratio A_t/A into Eq. (17) yields $\bar{\phi}$.

An analytical solution to Eq. (20) is still out of reach due to the complexity of the function $K(\psi, \zeta)$. It is possible to show that K is much more sensitive to variations in ζ than ψ. In fact, K varies by less than a factor of 2 along a ζ-surface. Thus, we approximate this function as constant with respect to ψ, from which we take the Taylor series of K and consider the limit as $\psi \to 0$. This procedure yields,

$$K(\psi, \zeta) \approx k(\zeta) = \frac{3\sqrt{2}}{8}\left[\frac{1 + 4\zeta}{\sqrt{\zeta(1 + 2\zeta)}}\right] \approx \frac{3}{4\sqrt{2\zeta}}, \tag{30}$$

where the approximation on the far-right-hand side is valid for $\zeta < 1$ (or, $z > 1$). Equations (16) and (20) thus give

$$\phi = \frac{1}{2}\left[1 - (1 - 2\bar{\phi})\frac{k\psi_p}{e^{k\psi_p} - 1} e^{k\psi}\right]. \tag{31}$$

We note that $\bar{M}^2 = 1 - 2\bar{\phi}$. Equation (31) then suggests that the extent to which non-uniformities manifest within the exhaust depends on the local, ψ-averaged ion Mach number. Indeed, we will show in Sec. IV that the relative focusing of the exhaust beam, and consequently the detachment of ions and beam divergence efficiency of the nozzle, both scale with $\bar{M}$.

The location at which 2D effects become important may be determined from the parameter,

$$\epsilon_u \equiv \left|\frac{\phi(\psi_p, \zeta) - \phi(0, \zeta)}{\bar{\phi}(\zeta) - \phi_e}\right| \approx 2k\psi_p\left[1 + \left(M_e/\bar{M}\right)^2\right]. \tag{32}$$

The approximation on the right-hand side is valid in the immediate expansion region ($k\psi_p \ll 1$). Setting $\epsilon_u = 0.05$ in

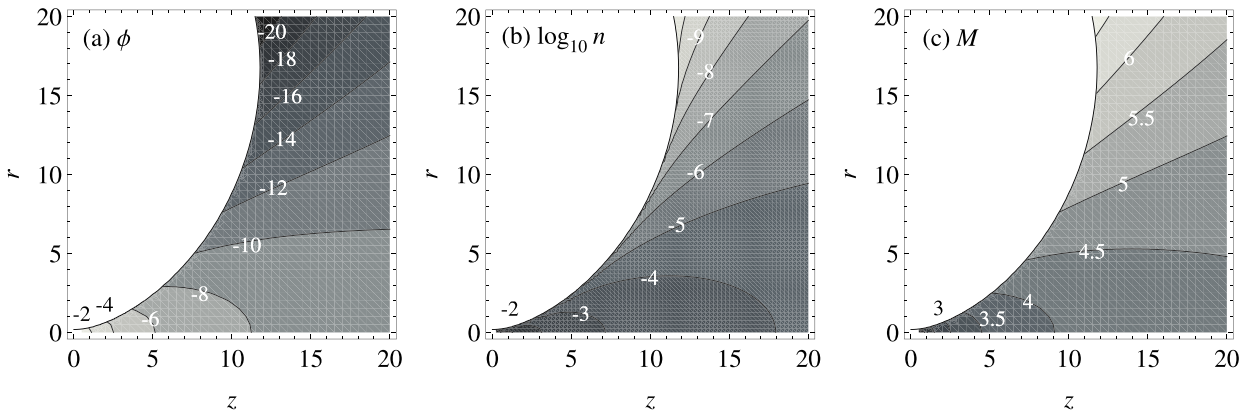

FIG. 4. Contour plots of the approximate analytical solution for the potential, ϕ, density, n, and ion Mach number, M, for the plasma exhaust plume of an ED-MN. The exhaust and throat planes coincide ($M_e = M_t = 1$), and the plasma radius at the exhaust plane is $r_e = 0.185$.

the limit $M_e/\bar{M} \ll 1$ yields $z^* \approx (2/30)r_e^{-2}$, where z^* is the axial location along the nozzle axis at which point 2D effects become predominant, which also corresponds to the breakdown of the self-similar assumption and the point at which ion detachment from the applied magnetic field begins. Clearly, z^* will increase for highly magnetized plasmas.

Closed-formed solutions for n and M are obtained by substituting Eqs. (28) and (31) into Eqs. (13) and (14). These expressions are not shown here for the sake of brevity. Finally, it may be necessary (e.g., to calculate C_T) to implement the mass-conservation correction outlined in Sec. II F. Numerical integration of Eq. (21) yields $\epsilon_{\dot{m}}$. Equations (23)–(25) can then be used to find α_ϕ, α_n, and α_M.

Contour plots of ϕ, n, and M are presented in Fig. 4 for $M_t = M_e = 1$ and $r_t = r_e = 0.185$. A number of observations may be made about the nature of this flow that are in qualitative agreement with the analysis of Ahedo and Merino:[6] (1) A large potential well develops along the plasma edge in the far field of the plume; (2) the increased potential gradient near the edge of the plume leads to a rarefaction of the plasma edge; and (3) ion acceleration near the nozzle axis is impeded in the far field region.

We show in Fig. 5 a quantitative comparison of our 2D separable solution to the numerical results of Ahedo and Merino. Specifically, we take sample points from the low magnetization ($\Omega_i = 0.1$) curve of Fig. 4 from Ref. 6 to compare the analytical and numerical solutions for the axial dependence of ϕ, n, and M along the nozzle axis, $\psi = 0$, and plasma edge, $\psi = \psi_p$. The dashed lines correspond to the solution without the mass conservation correction, while the solid lines include the correction.

A strikingly good agreement is found between our approximate, analytical solution and the numerical solution to the full two-fluid equations. Specifically, the analytical solution, both with and without the mass conservation correction, accurately tracks the non-uniformities in the potential and ion Mach number that develop in the downstream region. Furthermore, the increased rarefaction of the plasma along the boundary as predicted by the analytical solution matches that of the numerical solution. Finally, we note that $z^* = 1.95$ for this example, which coincides well with the location at which the two curves bifurcate in Fig. 5.

IV. THRUST AND EFFICIENCY MODEL

The main question presented in the Introduction may now be recast in terms of the specific parameters relevant to the 2D separable solution. Specifically, how does the beam divergence efficiency, η_{div}, and thrust coefficient, C_T, of an ED-MN depend on the normalized plasma radius, r_e, ion

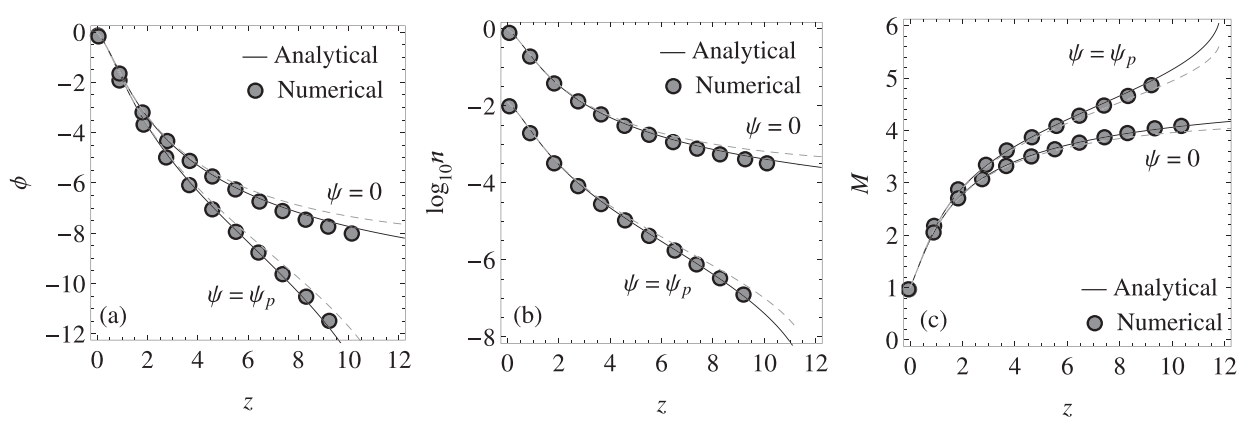

FIG. 5. Comparison of the approximate analytical solution with (solid) and without (dashed) the mass conservation correction for the potential, ϕ, density, n, and ion Mach number, M to the numerical results (shaded points) from Fig. 4 of Ref. 6. Note that the x-axis of the numerical data was adjusted to be consistent with our normalization.

Mach number, M_e, and density profile uniformity, σ, at the nozzle exhaust plane?

A. Model domain

It is necessary to first define the domain of our performance model. It is reasonable to suspect that the loss of magnetic confinement through plasma detachment defines the downstream boundary to the domain of a performance model. This is because the reaction force of the plasma on the MN results from the diamagnetic current, and this current is a by-product of confinement of the thermal plasma by the magnetic field. With that said, the process by which the plasma detaches from the MN is not fully understood and is a topic of active research.[28–32]

Fortunately, recent simulations of the far-field region of an ED-MN by Merino and Ahedo[52] show that a large portion (>99%) of the ion flow effectively separates from the applied magnetic field. In their model, the electrons are still confined by the magnetic field and continue to transfer momentum throughout the plume. Ion detachment implies that the bulk of the plasma, and thus the region that transfers the most momentum, continues to flow downstream as opposed to returning along the diverging magnetic field.

We conjecture, based on the results of Merino and Ahedo, that it is not necessary to include electron detachment within an ED-MN performance model as long as the solution captures the effects of ion detachment (specifically, the relative focusing of the plasma with respect to the applied field). Furthermore, the axial separation between the magnets and the far-field plasma implies that very little momentum is exchanged beyond the turning point of the applied magnetic field.

With this in mind, we define the domain for our performance model to be the volume of plasma up until the ζ-surface corresponding to the turning point of the nozzle, $\zeta_{\rm tp}$ (see Fig. 3). Effectively, we are assuming that electron detachment occurs downstream of $\zeta_{\rm tp}$. The performance parameters may then be obtained by considering the relevant momentum and power fluxes through the surface defined by $\zeta_{\rm tp}$. The algebraic complexity of the coordinate transformation precludes an analytical description of $\zeta_{\rm tp}$ as a function of ψ_p. However, $\zeta_{\rm tp}$ may be found numerically by solving $B_z(\psi_p, \zeta_{\rm tp}) = 0$. Fitting a curve to the various solutions, we obtain the relation, $\zeta_{\rm tp} \approx 2.5\psi_p^2$, which is accurate to within 8% for $\psi_p \in [0, 0.07]$.

B. Relative focusing and ion detachment

The plasma beam divergence will depend on the relative focusing of the plasma density profile in the plume with respect to the divergence of the applied magnetic field. As an index of this focusing, we derive here a scaling relation for the half-width at half-maximum of the plasma density profile at $\zeta_{\rm tp}$.

The normalized density profile at $\zeta_{\rm tp}$ is given by,

$$\chi_{\rm tp}(\Psi) = \frac{n(\Psi, \zeta_{\rm tp})}{n(0, \zeta_{\rm tp})}, \tag{33}$$

where $\Psi \equiv \psi/\psi_p$. The normalized half-width at half-maximum of the density profile at the nozzle turning point in the magnetic coordinate system, $\Psi_{1/2}$, may then be found from $\chi_{\rm tp}(\Psi_{1/2}) = 1/2$.

We find n using Eqs. (13) and (31), and approximate the plasma density profile at the throat, Eq. (28), as $n_t(\Psi) \approx 1 - [1 - J_0(a_0\sigma)]\Psi$. We substitute n into Eq. (33), expand $\chi_{\rm tp}(\Psi)$ in a Taylor series up to second order in Ψ, and solve for $\chi_{\rm tp}(\Psi_{1/2}) = 1/2$. From this procedure we find,

$$\Psi_{1/2} \approx \frac{1}{2}\left[f_b(\bar{M}_{\rm tp}, \sigma) - \sqrt{f_b(\bar{M}_{\rm tp}, \sigma)^2 - 4f_c(\bar{M}_{\rm tp}, \sigma)}\right], \tag{34}$$

where the functions f_b and f_c are given by

$$f_b(\bar{M}_{\rm tp}, \sigma) = \frac{1}{c_1\bar{M}_{\rm tp}^2} + \frac{1}{1 - J_0(a_0\sigma)}, \tag{35}$$

$$f_c(\bar{M}_{\rm tp}, \sigma) = \frac{1 - h_f/2}{[1 - J_0(a_0\sigma)]c_1\bar{M}_{\rm tp}^2}, \tag{36}$$

with constants,

$$c_1 = \frac{c_2^2}{2(e^{c_2} - 1)}, \quad c_2 = \frac{3}{4\sqrt{5}}. \tag{37}$$

Here, $\bar{M}_{\rm tp} = \bar{M}(\zeta_{tp})$ is the ψ-averaged Mach number at the nozzle turning point. The additional constant, h_f, accounts for higher order terms.

Equation (34) implies that $\Psi_{1/2}$ is dependent upon only two parameters: $\bar{M}_{\rm tp}$ and σ. Using the quasi-1D equations, $\bar{M}_{\rm tp}$ may be well-approximated as

$$\bar{M}_{\rm tp} \approx \sqrt{M_e^2 - 2\ln(5^{1/2}M_e\psi_p^3)}. \tag{38}$$

To verify the scaling of Eq. (34), we plot in Fig. 6 the numerical solution to Eq. (33) for $\Psi_{1/2}$ versus $\bar{M}_{\rm tp}$ for the following parameter space $\mathbb{P}$: $M_e \in [1, 4]$, $r_e \in [0.02, 0.45]$, and $\sigma \in [0.25, 1.0]$. We note that this parameter space will be used extensively throughout Sec. IV. Also shown in Fig. 6 are four curves that correspond to Eq. (34) with $\sigma = 0.25$, 0.5, 0.75, and 1.0. Here, $h_f = 1.22$ is chosen to produce the best fit.

The density profile HWHM *at the exhaust plane* may be approximately found by solving $J_0(a_0\sigma\sqrt{\Psi}) = 0.5$, which yields $\Psi \approx 6.4$, 1.6, 0.7, and 0.4 for $\sigma = 0.25$, 0.5, 0.75, and 1.0, respectively. It is clear from Fig. 6 that the HWHM at $\zeta_{\rm tp}$ is much less than its initial value, which indicates that the density profile has become focused with respect to the diverging magnetic field. Furthermore, this focusing increases with $\bar{M}_{\rm tp}$.

C. Performance scaling

We now use the results of Sec. IV B to derive scaling relations for $\eta_{\rm div}$ and C_T. Under the quasi-field-aligned assumption, the beam divergence efficiency may be written as,

$$\eta_{\rm div} \equiv \frac{\mathcal{P}_b^*}{\mathcal{P}_b} = \int_{\zeta_{\rm tp}} nM^3\frac{B_z^2}{B^2}dA \Big/ \int_{\zeta_{\rm tp}} nM^3 dA. \tag{39}$$

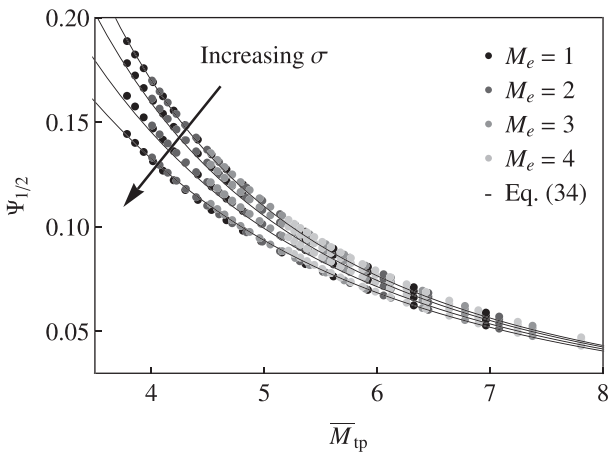

FIG. 6. Half-width at half-maximum of the normalized density profile, $\Psi_{1/2}$, versus the ψ-averaged Mach number, $\bar{M}_{tp}$, at ζ_{tp}. Data points are found from the numerical solution of $\chi_{tp} = 1/2$. The analytical model (solid line) comes from Eq. (34).

Unfortunately, even though we now have analytical equations for the 2D distributions of each plasma parameter, the above integrals do not yield simple closed-form solutions. Therefore, η_{div} must be found through numerical integration of Eq. (39).

It is reasonable to assume, however, that the beam divergence efficiency may scale with the HWHM of the plasma density profile. As $\Psi_{1/2}$ decreases, we anticipate the beam divergence efficiency to increase because more plasma is concentrated along the nozzle axis. We take the effective plume half-angle, θ_{div}, to be the angle that the magnetic field vector makes with the nozzle centerline at $\Psi_{1/2}$. This may be approximated as $\cos\theta_{div} \approx 1 - \Psi_{1/2}$. The beam divergence efficiency should then scale as $\eta_{div} \sim (1 - \Psi_{1/2})^2$. Indeed, Fig. 7 shows that this scaling is valid for small $\Psi_{1/2}$.

Adding a term to correct for larger values of $\Psi_{1/2}$, we propose the following model for η_{div}:

$$\eta_{div} \approx c_{\eta 1}[(1 - \Psi_{1/2})^2 - 1] + c_{\eta 2}\Psi_{1/2}^2 + 1. \tag{40}$$

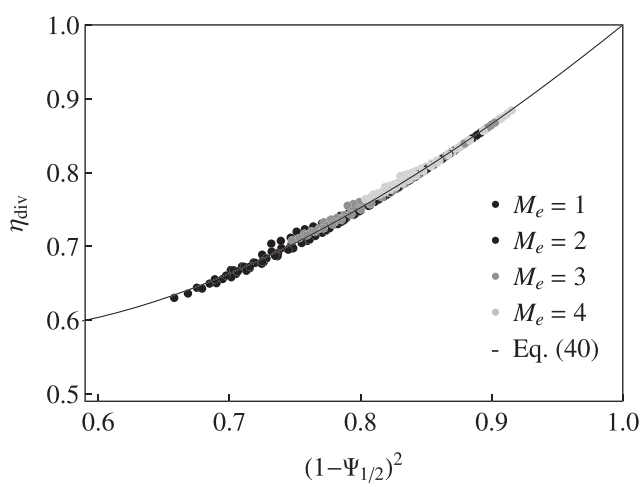

FIG. 7. Beam divergence efficiency, η_{div}, versus the quantity $(1 - \Psi_{1/2})^2$. Data points are found from the numerical solution of Eq. (39) in the parameter space $\mathbb{P}$. The analytical solution (solid line) comes from Eq. (40).

Here, $c_{\eta 1} = 1.432$ and $c_{\eta 2} = 3.473$ result from the method of least-squares. Equation (40), with $\Psi_{1/2}$ found from Eqs. (34) and (38), represents a fully analytical equation for the beam divergence efficiency of an ED-MN in terms of M_e, r_e, and σ.

Fig. 8 shows the beam divergence efficiency versus the normalized plasma radius for four different values of the ion Mach number at the exhaust plane and $\sigma = 1$. Similar agreement between the numerical solution to Eqs. (39) and (40) may be seen for different values of σ. We can summarize from these plots the general dependence of the beam divergence efficiency on the nature of the exhaust plane plasma:

1. η_{div} decreases as r_e increases, and is very sensitive to changes in r_e.
2. The increased η_{div} that results from increasing M_e becomes more pronounced for $M_e > 1$ and $r_e > 0.1$.
3. Decreases in σ lead to decreases in η_{div} (not shown).
4. The sensitivity of η_{div} to changes in σ is much greater for small M_e (not shown).

Each of these dependencies is predicted by Eqs. (34), (38), and (40) over the chosen parameter space. We note that the first and third dependencies were first observed in the numerical results of Ahedo and Merino.[6]

We now consider the thrust coefficient, C_T. Earlier we defined the thrust coefficient as the thrust divided by the pressure force of the plasma at the nozzle throat. Within the quasi-field-aligned framework this may be written as,

$$C_T = \frac{1}{\bar{n}_t A_t}\int_{\zeta_{tp}} n(M^2 + 1)\frac{B_z}{B}dA. \tag{41}$$

Here, we take the thrust to be equal to the momentum flux through the surface ζ_{tp}.

We note that C_T represents the thrust coefficient of the entire magnetic nozzle. Because we assume the flow is choked, C_T is independent of the internal thermal energy of the plasma. The thrust coefficient contribution of the plasma upstream of the exhaust plane is equal to $M_e + 1/M_e$, where the first and second terms represent the ion kinetic and electron thermal momentum flux contributions, respectively.

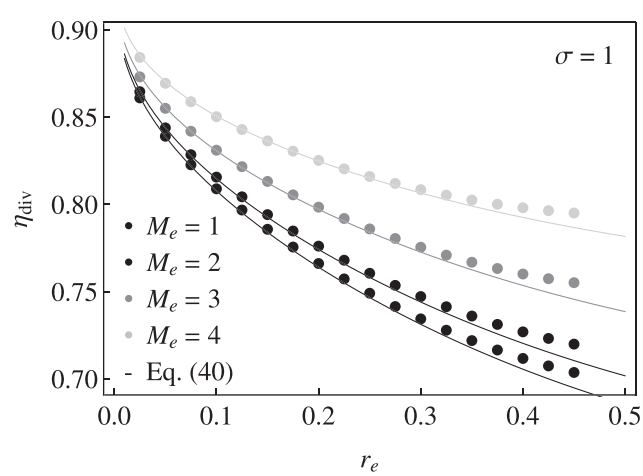

FIG. 8. Beam divergence efficiency, η_{div}, versus the normalized exhaust radius, r_e, for $\sigma = 1$ and $M_e \in [1, 4]$. Data points are found from the numerical solution of Eq. (39). The analytical solution (solid lines) comes from Eq. (40).

For $M_e = 1$, only half of the internal energy has been converted into kinetic energy at the exhaust plane, and a sizable portion of the thrust is generated in the exhaust region.

It can be noted that $C_T \to \infty$ as $M_e \to \infty$. However, this limit implies through Eq. (29) that $R_E \to \infty$, which is clearly unphysical. Furthermore, M_e is relatively insensitive to large increases in R_E for $M_e > 4$. Thus, the $M_e \gg 1$ limit is not relevant to our model.

We anticipate that the thrust coefficient will exhibit some dependence on η_{div}. We characterize this dependence in Fig. 9 by plotting the numerical solutions for C_T versus η_{div} for $\sigma = 1$. It is clear from this figure that C_T increases with η_{div}. This indicates that, for a fixed throat pressure, the thrust increases as the beam divergence decreases. Furthermore, C_T exhibits a linear relationship with η_{div}, with the proportionality constants depending on M_e. It can be shown that the constants of proportionality also depend on σ.

Therefore, we construct the following model for C_T:

$$C_T = f_1(M_e, \sigma)\eta_{\text{div}} + f_2(M_e, \sigma), \tag{42}$$

$$f_2(M_e, \sigma) = q_1(\sigma)M_e^2 + q_2(\sigma)M_e + q_3(\sigma), \tag{43}$$

$$f_1(M_e, \sigma) = q_4(\sigma)f_2(M_e, \sigma) + q_5(\sigma). \tag{44}$$

It may be shown that $q_j(\sigma)$ is approximately quadratic in σ, such that

$$q_j(\sigma) = \sum_{k=0}^{2} q_{jk}\sigma^k. \tag{45}$$

Fifteen coefficients are required to solve for C_T in Eq. (42). We obtain these coefficients by taking the numerical solution to Eq. (41) over the parameter space $\mathbb{P}$ and performing a least-squares fit to the above model. These are tabulated in Table I. Plots of Eq. (42) using the coefficients in Table I may be seen in Fig. 9 for $\sigma = 1$.

The thrust coefficient dependence on the exhaust plane plasma radius for various Mach numbers is shown in Fig. 10 for $\sigma = 1$. From this figure, we see that the dependence of C_T on the different exhaust plane plasma parameters is very similar to the dependence that we summarized above for η_{div}. With that said, we do note one exception: unlike for η_{div}, C_T maintains approximately the same sensitivity to M_e regardless of the value of r_e/a_e. This is because the constant of proportionality between C_T and η_{div} depends on M_e.

TABLE I. Least-squares coefficients for Eq. (45).

$k =$	0	1	2
q_{1k}	−1.010	−0.574	0.520
q_{2k}	2.287	0.928	−1.024
q_{3k}	−10.223	4.062	−6.616
q_{4k}	−1.214	−0.002	0.024
q_{5k}	6.602	0.278	−0.216

The form of Eqs. (39) and (41) inherently assumes that the ion velocity vector is aligned with the local magnet field vector at the nozzle turning point. The error due to this assumption leads to η_{div} and C_T values lower than would be predicted if the slip angle of the ion velocity vector were included. We analyze the effect of this error by assuming a slip angle between the two vectors at ζ_{tp} of the form $\delta = \delta_m \sin(\pi\Psi/2)$, where δ_m is the maximum slip angle. Including the slip angle within the η_{div} and C_T equations, it is possible to show that the error in Eqs. (39) and (41) scale according to $\epsilon_\eta \sim 2\delta_m(1-\eta_{\text{div}})^{3/2}$ and $\epsilon_{C_T} \sim 0.35\delta_m(1 - C_T/10)^2$, respectively. ϵ_η remains less than 5% for $r_e \leq 0.15$ and $\delta_m \leq 15°$. As r_e increases, however, ϵ_η can rise up to 10% for $\delta_m = 15°$. To good approximation, $\epsilon_{C_T} \sim \epsilon_\eta/2$.

Our analytical solution prevents a consistent description of δ_m because of the limitations of the quasi-field-aligned approximation. As a result, the performance model derived in this section underpredicts η_{div} and C_T by an error that scales according to ϵ_η and ϵ_{C_T}, respectively. While this error remains low for C_T, a semi-empirical correction that accounts for the ion slip angle is needed to improve the accuracy of the η_{div}-model for $\eta_{\text{div}} \lesssim 0.80$. However, the general scaling of η_{div}, shown in Fig. 8, remains unchanged with the

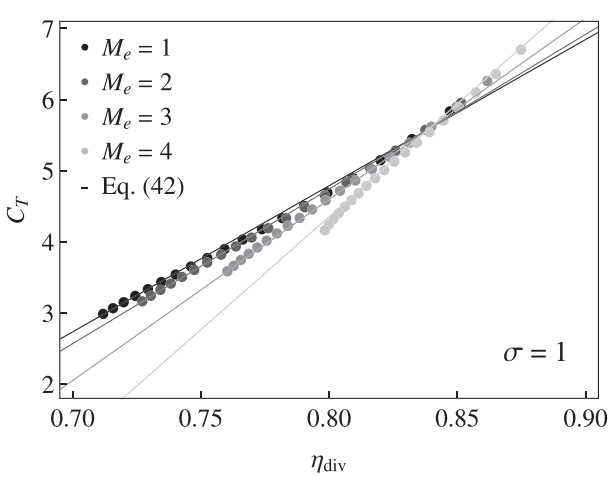

FIG. 9. Linear relationship between C_T and η_{div}. Data points are found from the numerical solution of Eqs. (39) and (41). The analytical model (solid lines) results from Eq. (42).

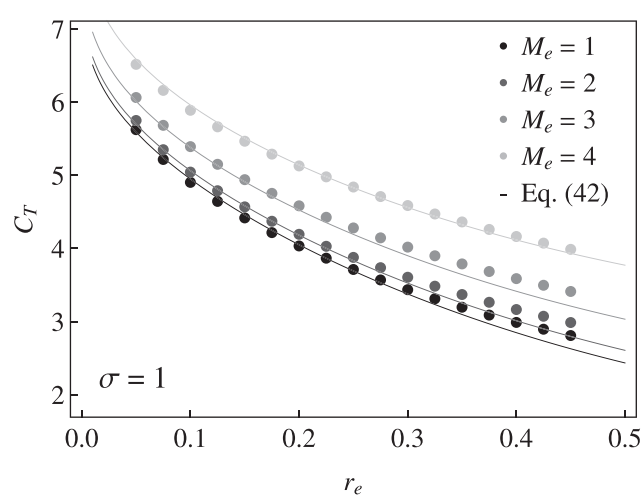

FIG. 10. Thrust coefficient, C_T, versus the normalized exhaust radius, r_e, for $\sigma = 1$. Data points are found from the numerical solution of Eq. (41). The analytical model (solid lines) results from Eq. (42).

exception that the curves are translated upward by a factor proportional to δ_m. Therefore, the qualitative trends observed in this section remain valid for finite δ_m.

D. Nozzle design implications

Most ED-MN thrusters that have been built in the laboratory utilize the fringe fields of the plasma source as a simple MN. The results of Sec. IV C allow us to compare the performance of the more general MN configuration depicted in Fig. 1 with the simple MN. Specifically, we want to answer the question: *how is the divergence efficiency of an ED-MN affected by the addition of an acceleration region?*

We showed in Sec. III B that the ion Mach number and plasma radius at the exhaust section may be adjusted by altering the MN geometry. Specifically, M_e is determined by the expansion ratio from Eq. (29). Using the simple two magnet configuration depicted in Fig. 1, the normalized plasma radius at the exhaust, $r_e = R_{a,e}^{1/2}$, is related to the aperture ratio at the throat of the nozzle and the expansion ratio through

$$\frac{R_{A,e}}{R_{A,t}} \approx R_E \left(\frac{a_t}{a_e}\right)^2 \approx \frac{1}{R_E}\left(\frac{I_t}{I_e}\right)^2. \tag{46}$$

Here, $I_t = a_t B_t$ and $I_e = a_e B_e$ represent the effective total current needed to produce the magnetic field B_t and B_e for the throat and exhaust magnets, respectively.

We may use Eq. (46) to examine the effect of adding an acceleration region to a given thruster. It is clear that R_A decreases with increasing R_E if the exhaust magnet carries the same current as the throat magnet, but at a larger radius. Alternatively, R_A increases with R_E if the exhaust magnet, while carrying less current, is the same size as the throat magnet.

Because η_{div} increases as R_A decreases, it is not beneficial to add an exhaust magnet that is the same size as the throat magnet. The addition of an exhaust magnet that is larger than the throat magnet, yet carrying comparable current, does lead to increased performance. However, it can be shown that this increase in performance is only significant for plasmas in which the throat aperture ratio is relatively large ($R_{A,t} \gtrsim 0.2$). This relates to our previous observation that improvements in η_{div} become more sensitive to increases in M_e as r_e increases.

In general, the addition of an acceleration region adds weight and complexity to the thruster. Equation (46) implies that an exhaust magnet may only be beneficial for thrusters that exhibit poor confinement near the throat (large $R_{A,t}$). This may change, however, for highly magnetized plasmas ($\rho_i \ll 1$). The desire to reduce losses within the plasma source may lead to magnetic fields much larger than those reported in the literature for ED-MN thrusters. Plasma flow from an ED-MN in the high magnetization limit has been marked by a noticeable decrease in performance.[6,52] Therefore, substantial efficiency improvements may be seen by using an exhaust magnet to step down the effective level of ion magnetization prior to exiting the thruster. A full analysis of this problem, however, is beyond the scope of this paper.

V. CONCLUSIONS

An approximate, fully analytical solution to a two-fluid model of plasma flow along an applied magnetic field has been derived to aid performance modeling of propulsion plasmas. The model is relevant to collisionless plasmas with cold ions and isothermal electrons. It was applied to the problem of plasma expansion through a magnetic nozzle, from which excellent agreement was found between our analytical solution and the numerical solution[6] to the same model.

From our analytical solution, scaling relations for the beam divergence efficiency and thrust coefficient of an ED-MN were derived. It was found that these performance parameters depend on the ion Mach number, normalized plasma radius, and density profile uniformity at the nozzle exhaust plane. Improved performance is predicted for small plasma radii with density profiles that are peaked on the nozzle axis because the effective divergence of the applied magnetic field is lower in this region, which agrees with the numerical simulations of Ahedo and Merino.[6] Additionally, high exhaust Mach numbers increase the performance by decreasing the divergence losses of the exhaust beam. We conclude from these observations that the addition of an acceleration region to allow for high Mach number exhaust flow is only beneficial if it also decreases the plasma radius relative to the exhaust magnet radius.

Omissions from the 2D performance model include the magnetic force on the ions and electron detachment from the applied magnetic field. Numerical simulations imply that the magnetic force on ions may be neglected for ED-MN plasmas of similar properties to those in the literature.[6] If the magnetic field strength is substantially increased, which may be necessary to improve the performance of these thrusters by limiting energy losses within the plasma source,[41] then the magnetic force should be taken into account within the performance model. Furthermore, it is possible that electron detachment occurs prior to the nozzle turning point. Two such mechanisms by which this detachment may occur are the demagnetization of the electrons due to finite Larmor radius effects[29,32] or induced magnetic field effects.[13,31,49] It is predicted that both of these effects increase the divergence of the plasma and lead to decreased performance.[31,32] Incorporating these effects within an analytical model has proven to be quite complex, and will likely need further assistance from experimental observations and computational modeling.

ACKNOWLEDGMENTS

The first author was supported by the Department of Defense (DoD) through the National Defense Science & Engineering Graduate Fellowship (NDSEG) Program. We thank the Program in Plasma Science and Technology for support through DOE Contract No. DE-AC02-09CH11466. We also thank Professor E. Ahedo and M. Merino for insightful discussion.

[1] I. Podgornyi and R. Z. Sagdeev, Sov. Phys. Usp. **12**, 445 (1970).
[2] W. M. Manheimer and R. F. Fernsler, IEEE Trans. Plasma Sci. **29**, 75 (2001).

[3]G. R. Seikel, *Electric Propulsion for Spacecraft* (1962), Vol. 22, p. 19.
[4]K. Kuriki and O. Okada, Phys. Fluids **13**, 2262 (1970).
[5]E. L. Walker and G. R. Seikel, "Axisymmetric expansion of a plasma in a magnetic nozzle including thermal conduction," Technical Report No. TN D-6154, NASA, 1971.
[6]E. Ahedo and M. Merino, Phys. Plasmas **17**, 073501 (2010).
[7]E. Ahedo, Plasma Phys. Controlled Fusion **53**, 124037 (2011).
[8]E. Ahedo, Phys. Plasmas **18**, 033510 (2011).
[9]M. Merino and E. Ahedo, Phys. Plasmas **20**, 023502 (2013).
[10]D. Miller and G. W. Bethke, AIAA J. **4**, 932 (1966).
[11]J. C. Sercel, "An experimental and theoretical study of the ECR plasma engine," Ph.D. thesis, (Cal. Tech., Pasadena, CA, 1993).
[12]B. Stallard, E. Hooper, and J. Power, J. Propul. Power **12**, 814 (1996).
[13]R. Winglee, T. Ziemba, L. Giersch, J. Prager, J. Carscadden, and B. Roberson, Phys. Plasmas **14**, 063501 (2007).
[14]D. Pavarin, F. Ferri, M. Manente, D. Curreli, D. Guclu, Y. Melazzi, D. Rondini, S. Suman, J. Carlsson, C. Bramanti, E. Ahedo, V. Lancellotti, K. Katsonis, and G. Markelov, in *Proceedings of the 31st International Electric Propulsion Conference, Ann Arbor, MI*, Paper No. 205 (Electric Rocket Propulsion Society, Fairview Park, OH, 2009).
[15]S. Pottinger, V. Lappas, C. Charles, and R. Boswell, J. Phys. D: Appl. Phys. **44**, 235201 (2011).
[16]K. Takahashi, T. Lafleur, C. Charles, P. Alexander, and R. W. Boswell, Phys. Rev. Lett. **107**, 235001 (2011).
[17]L. T. Williams and M. L. R. Walker, J. Propul. Power **29**(3), 520 (2013).
[18]A. Shabshelowitz and A. D. Gallimore, J. Propul. Power **29**(4), 919 (2013).
[19]S. A. Cohen, N. Siefert, S. Stange, R. Boivin, E. Scime, and F. Levinton, Phys. Plasmas **10**, 2593 (2003).
[20]B. W. Longmier, L. D. Cassady, M. G. Ballenger, M. D. Carter, F. R. Chang-Diaz, T. W. Glover, A. V. Ilin, G. E. McCaskill, C. S. Olsen, and J. P. Squire, J. Propul. Power **27**, 915 (2011).
[21]I. G. Mikellides, P. G. Mikellides, P. J. Turchi, and T. M. York, J. Propul. Power **18**, 152 (2002).
[22]J. M. Little, A. S. Rubin, and E. Y. Choueiri, in *Proceedings of the 32nd International Electric Propulsion Conference, Wiesbaden, Germany*, Paper No. 2011–229 (Electric Rocket Propulsion Society, Fairview Park, OH, 2009).
[23]J. E. Polk, W. v. Jaskowsky, A. J. Kelley, and R. G. Jahn, J. Propul. Power **3**, 33 (1987).
[24]I. G. Mikellides, I. Katz, and R. R. Hofer, "*Design of a Laboratory Hall Thruster with Magnetically Shielded Channel Walls, Phase I: Numerical Simulations*," AIAA Paper 2011–5809.
[25]R. R. Hofer, D. M. Goebel, I. G. Mikellides, and I. Katz, "*Design of a Laboratory Hall Thruster with Magnetically Shielded Channel Walls, Phase II: Experiments*," AIAA Paper 2012–3788.
[26]I. G. Mikellides, I. Katz, R. R. Hofer, and D. M. Goebel, "*Design of a Laboratory Hall Thruster with Magnetically Shielded Channel Walls, Phase III: Comparison of Theory with Experiment*," AIAA Paper 2012–3789.
[27]A. Schwabedissen, E. C. Benck, and J. R. Roberts, Phys. Rev. E **55**, 3450–3459 (1997).
[28]R. W. Moses, Jr., R. A. Gerwin, and K. F. Schoenberg, AIP Conf. Proc. **246**, 1293 (1992).
[29]E. B. Hooper, J. Propul. Power **9**, 757 (1993).
[30]A. V. Arefiev and B. N. Breizman, Phys. Plasmas **12**, 043504 (2005).
[31]E. Ahedo and M. Merino, Phys. Plasmas **18**, 053504 (2011).
[32]E. Ahedo and M. Merino, Phys. Plasmas **19**, 083501 (2012).
[33]R. Comfort, "Modeling magnetospheric plasma," Geophys. Monogr. **44**, 51 (1988).
[34]B. W. Longmier, E. A. Bering III, M. D. Carter, L. D. Cassady, W. J. Chancery, F. R. C. Díaz, T. W. Glover, N. Hershkowitz, A. V. Ilin, G. E. McCaskill *et al.*, Plasma Sources Sci. Technol. **20**, 015007 (2011).
[35]C. Charles, Plasma Sources Sci. Technol. **16**, R1 (2007).
[36]A. B. Sefkow and S. A. Cohen, Phys. Plasmas **16**, 053501 (2009).
[37]E. Ahedo and M. Martínez Sánchez, Phys. Rev. Lett. **103**, 135002 (2009).
[38]N. Singh, Phys. Plasmas **18**, 122105 (2011).
[39]C. Charles and R. Boswell, Phys. Plasmas **11**, 1706 (2004).
[40]R. G. Jahn, *Physics of Electric Propulsion* (McGraw-Hill, Inc., New York, 1968).
[41]E. Ahedo, in *Proceedings of the 31st International Electric Propulsion Conference, Ann Arbor, MI*, Paper No. 193 (Electric Rocket Propulsion Society, Fairview Park, OH, 2009).
[42]D. A. Carl, M. Williamson, M. Lieberman, and A. Lichtenberg, J. Vac. Sci. Technol. B **9**, 339 (1991).
[43]A. Ellingboe and R. Boswell, Phys. Plasmas **3**, 2797 (1996).
[44]C. M. Franck, O. Grulke, and T. Klinger, Phys. Plasmas **10**, 323 (2003).
[45]S. Andersen, V. O. Jensen, P. Nielsen, and N. D'Angelo, Phys. Fluids **12**, 557 (1969).
[46]D. L. Chubb, AIAA J. **10**, 113 (1972).
[47]G. I. Dimov and S. Y. Taskaev, in *Proceedings of the 27th EPS Conference on Controlled Fusion and Plasma Physics, Budapest, Hungary* (American Institute of Aeronautics and Astronautics, Washington, DC, 2000), ECA Vol. 24B, pp. 464–467.
[48]A. Fruchtman, K. Takahashi, C. Charles, and R. Boswell, Phys. Plasmas **19**, 033507 (2012).
[49]A. V. Arefiev and B. N. Breizman, Phys. Plasmas **15**, 042109 (2008).
[50]C. A. Deline, R. D. Bengtson, B. N. Breizman, M. R. Tushentsov, J. E. Jones, D. G. Chavers, C. C. Dobson, and B. M. Schuettpelz, Phys. Plasmas **16**, 033502 (2009).
[51]K. Takahashi, Y. Itoh, and T. Fujiwara, J. Phys. D: Appl. Phys. **44**, 015204 (2011).
[52]M. Merino and E. Ahedo, "*Magnetic Nozzle Far-Field Simulation*," AIAA Paper No. 2012–3843.
[53]F. F. Chen and M. A. Lieberman, *Introduction to Plasma Physics and Controlled Fusion* (Plenum Press, New York, 1984).
[54]T. Sakurai, Space Sci. Rev. **51**, 11 (1989).
[55]E. Ahedo, Phys. Plasmas **16**, 113503 (2009).
[56]R. A. Gerwin, "Integrity of the plasma magnetic nozzle," Technical Report No. TP-2009-213439, NASA, 2009.